Global Advanced Research Journal of Microbiology (ISSN: 2315-5116) Vol. 7(1) pp. 006-022, February, 2018 Issue.
Available online http://garj.org/garjm

Full Length Research Paper

Bioremediation of Methyl Orange onto *Nostoc carneum* Biomass by Adsorption; Kinetics and Isotherm Studies

Mervat H. Hussein*, Ghada S. Abou El-Wafa, Sami A. Shaaban-Dessuki and Rehab M. El-Morsy

Botany Department, Faculty of Science, Mansoura University, Mansoura, Egypt

Accepted 08 February, 2018

The present study is concerning with the use of cyanobacterium *Nostoc carneum* as a model for potential biosorbent of azo dye Methyl Orange (MO) from aquatic solutions. The impacts of major variables (pH, contact time, initial dye concentration, biosorbent capacity and salt concentrations) overriding algal biosorbent and process settings on specific decolorization rate and dye biosorbtion were investigated. Michaelis–Menten kinetics model was applied to assess the decolorization kinetics factors as 2.173 mg g^{-1} h^{-1} and 46.435 mg L^{-1} for maximum specific decolorization rate and k_m of dye concentration, respectively. The adsorption of MO is increasing with increasing the initial dye concentration as well as the algal biosorbent. *Nostoc carneum* with decolorization efficiency 50.749, 44.225, 42.934, 38.367, 36.211, 28.056, 23.754, 18.273 and 17.241 % at dye concentrations of 5, 10, 20, 30, 40, 50, 60, 70 and 80 mg L^{-1}, respectively at contact time 5 h. The maximum specific decolorization rate was found to be 2.1734 mg g^{-1} h^{-1}. Pseudo-second order kinetic rate and Langmuir adsorption isotherm models were the best fitted with the experimental equilibrium data. The interaction of MO with the biosorbent was demonstrated on the bases of scanning electron microscopy (SEM), FT-IR and XRD spectral data that prove the efficiency of *Nostoc carneum* fresh biomass with respect to alternative low-cost technology for azo dyes bioremediation.

Keywords: *Nostoc carneum*; Azo dye; Methyl orange; Biosorption kinetics; Isotherms; SEM; XRD; FTIR

INTRODUCTION

Azo dyes are assumed to be the major group of the industrial dyes production (60–70 %), that being commonly used as synthetic dyes in textile, food, paper and cosmetics because of their ease and cost-effectiveness compared with natural dyes as reported by Ong et al. (2010).

However, release of residual azo dye into the industrial effluents deteriorates the water quality with hazard impact on public health based on the azo dye structures, toxicity and carcinogenic potentiality (Heiss et al., 1992). The structural similarity that characterizes azo dyes is the presence of at least one R–N=N-R' group. The R and R' components of the azo functional group can be either aryl or alkyl groups (Daneshvar et al., 2007). The azo bonds are hardly removed because of their high water solubility as well as low exhaustion with the potential for persistence and accumulation in the environment (Pinheiro et al., 2004).

*Corresponding Author's Email: mervathussein56@yahoo.com

MO serves as a pollutant dye for the common water-soluble azo dyes being widely used in industries (Rakhshaee et al., 2011). Thus, the removal of them from industrial wastewaters is capital with regard to protect public health, environment, and aquatic life.

Microalgae are characterized by their quick reply to environmental variations according to their rapid growth rate contrasted to higher plants. They possess high surface area to volume ratio imparting significant potential for biosorption. Moreover, they are the natural habitants of oxidation pond of wastewater treatment plants as demonstrated by Mohan et al. (2004). *Chlorella vulgaris, Chlorella pyrenoidosa*, *Spirogyra* sp., *Oscillatoria tenuis, Oscillatoria rubescens* and *Elakatothrix viridis* can reduce azo dyes depending on their molecular structure and algal species (El-Sheekh et al., 2009; Jinqi and Houtian, 1992; Omar, 2008).

Ho (2006) indicated that the best suitable kinetic rate equation must be estimated by linear regression, through batch experiments at different initial sorbate concentrations, sorbent dosages, agitation speeds, pH values and temperatures as well as both sorbent and sorbate types.

Therefore, the main objectives of this study are to

i. evaluate the potential of *Nostoc carneum* for Methy Orange (MO) decolorization,

(ii) evaluate various physicochemical controlling factors affecting adsorption including pH, dye concentrations, biosorent dosage, salt concentrations and contact time,

ii. stat the kinetic parameters for explaining the nature of adsorption process, and

(iv) define the practicality isotherm model for the best-fit isotherm equation.

These data could be useful for further research and the practical applications of algal biosorbent in the dyeing wastewater treatment.

MATERIALS AND METHODS

Biosorbent

Fresh biomass of the cyanobacterium *Nostoc carneum* grown in BG11 medium (Stanier et al., 1971) was used as a biosorbent for studying MO decolorization. Algal cells were harvested at the beginning of stationary phase (18^{th} day).

Adsorbate

MO (4-[4-(dimethyl amino) phenylazo] benzene sulfonic acid), is a sulfonated mono-azo dye having molecular formula $C_{14}H_{14}N_3NaO_3S$ was selected as an adsorbate (model dye). It forms orange crystals and is used as an acid-base indicator. The dye stock solution was adjusted to the concentration 100 mg/l.

Adsorption equilibrium experiments

Adsorption equilibrium studies using batch technique were applied. 125 ml solutions of 50 mg l^{-1} of MO, as the initial concentration, in 250 ml Erlenmeyer flask were treated with the corresponding fresh biomass to the following doses: 1.6, 2.4, 3.2 and 4 mg *Nostoc carneum* dry biomass, respectively. The experimental flasks were agitated horizontally at 200 rpm for 5 h at room temperature, followed by centrifugation at 4.0×10^3 rpm (10 min) in order to separate phases. All runs were performed in triplicate and the standard error was calculated. Control flasks (without algal cells) were simultaneously used to confirm sorption potentiality of *N. carneum*. Residual dye concentrations were analyzed using a Unico UV-2000 Spectrophotometer. The absorbance was measured at the maximum wavelength of the MO dye (λ_{max} = 470 nm) using scan spectrophotometer Unican UV/Vis (England) as illustrated by Figure. 1 (a) and the dye concentrations were calculated through a standard curve. The samples were discarded with time course intervals up to 5 h.

The decolorization efficiency (DE) was calculated as the dye percentage that was declined from the solution through biosorption process according to Chen and Lin (2007).

$$DE = \frac{C_i - C_e}{C_e} \times 100 \quad (1)$$

Where C_i is the initial dye concentrations and C_e is the equilibrium dye concentrations. The specific decolorization rate (SDR) was estimated by eq. 2.

$$SDR = \frac{1}{c} \times \frac{\Delta[dye]}{\Delta t} \quad (2)$$

Where C is the biomass concentration (g dry wt. L^{-1}), [dye] the adsorbed dye concentration (mg L^{-1}), and t is the incubation time (h). SDR_{max} can be determined by plotting 1/SDR vs. $1/C_0$ as in Michaelis–Menten model (Chen and Lin, 2007). The Michaelis constant for initial dye concentration (Km) corresponds to *y*-intercept × slope and the *y*-intercept corresponds to $1/SDR_{max}$.

Adsorption rate experiments

For kinetic studies, a batch experiment was conducted. Solutions of 5, 10, 20, 30, 40, 50, 60, 70 and 80 mg L^{-1} MO, as the initial concentration, were treated with fresh biomass corresponding to 2.4 mg dry biomass at room temperature. The experimental flasks were agitated horizontally at 200 rpm. Representative samples were taken at time periods of (1, 2, 3, 4 and 5 h).

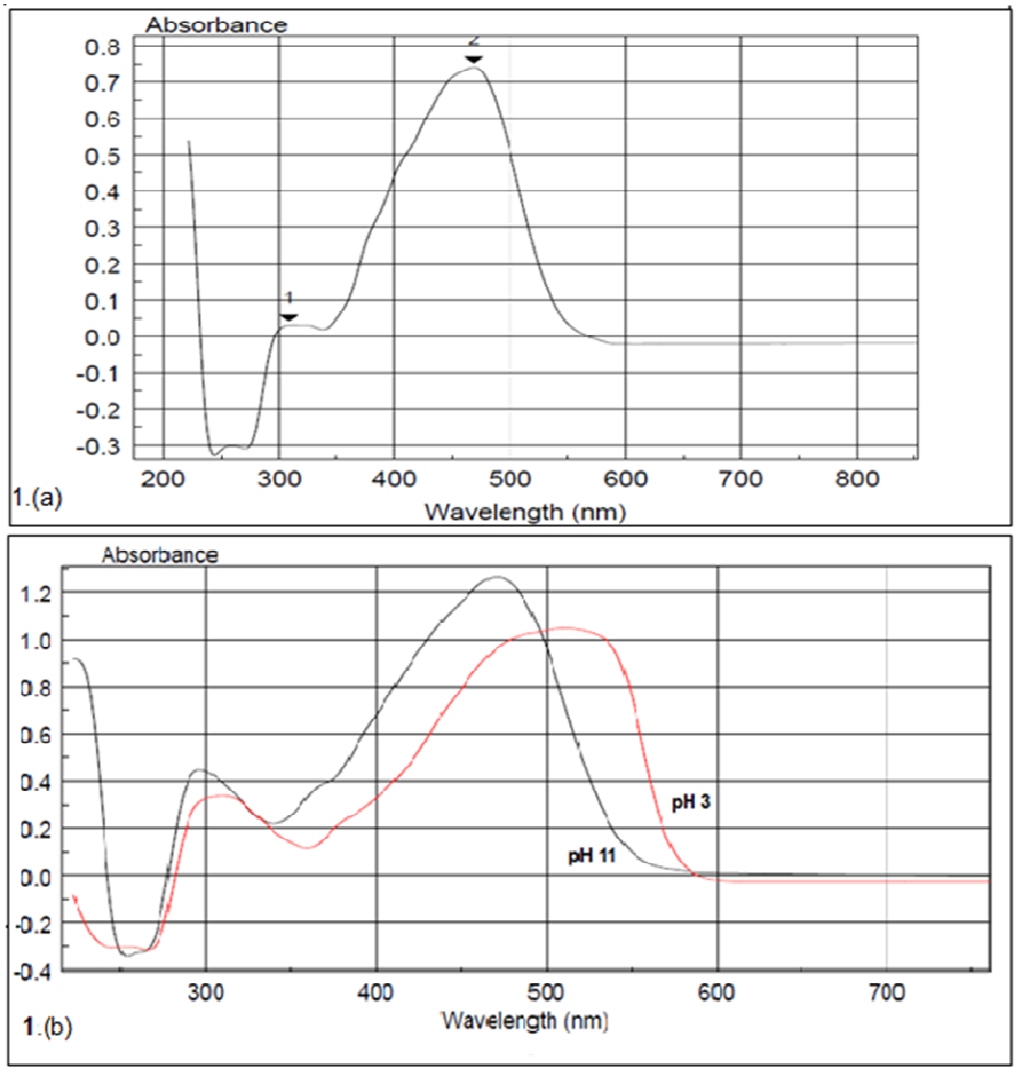

Figure 1 UV-vis. absorption spectra of methyl orange solution at (a) pH 7 and (b) pH 3 and pH 11

Effect of pH

In order to study the influence of various pH values on MO biosorption using *N. carneum* fresh biomass corresponding to 2.4 mg dry biomass was added to solutions containing 50 mg L^{-1} of MO ions. The initial pH values were adjusted at 3, 7 and 11 using 1.0 N HCl and 1.0 N NaOH. After the suspensions were shaken for 5 h. The algal biomass loaded with MO was centrifuged at 4.0 x 10^3 rpm for adsorbate separation. In case of pH 3 and pH 11, the absorbance was measured at λ_{max} = 510 nm and λ_{max} = 470 nm respectively, using scan spectrophotometer Unican UV/Vis (England) as illustrated in Figure. 1(b).

Effect of salt concentration

Effect of salt concentration had been studied using different concentrations of sodium chloride solutions (17, 34, 51, 68 and 85 mM) in addition of 50 mg L^{-1} dye solution. Residual dye concentrations were determined as mentioned above.

Characterization of *N. carneum* biosorbent

Biosorbent surface topography was examined before and after adsorption using scanning electron microscopy (SEM; JEOL JSM 6510N, Japan) at the Unit of Electron Microscope - Mansoura University. XRD spectra were

obtained using X-Pert Pro Diffractomerter having CuKα (k=1.54 Aº) radiation and programmable divergence slit. The voltage and current of the X-ray source were 40 KV and 20 mA. Dried sample was mounted on a silica plate and the intensity peaks of the diffracted X-rays were documented with time intervals 1 second at 25º C with monitoring the diffraction angle from 4º to 80º (2Θ). FT-IR spectroscopy was used to investigate the vibrational frequency changes in the cyanobacterial biosorbent, using Shimadzu FT-IR-84005 spectrometer within the range 4000 cm^{-1} at a resolution of 1 cm^{-1}. Zeta potential value for cyanobacterial extract is determined using Zeta potential analyzer (Malven Zeta size Nano-Zs90 – Unit of Electron Microscope - Mansoura University).

Adsorption isotherms and kinetic models

Kinetic models

The adsorption kinetics demonstrates the development of the adsorption potentiality during time and its necessity for recognizing the categories of adsorption mechanism in the biosorption process. The following models are applied to illustrate the adsorption kinetics behaviour:

Pseudo-first and pseudo-second order models

According to Lagergren suggestion of the pseudo-first order adsorption kinetics was described by Azizian (2004) in eq. 3.

$$\frac{dq}{dt} = k_1(q_e - q_t) \quad (3)$$

Where; K_1 (min^{-1}) is the constant rate of pseudo-first order model, q_t (mg g^{-1}) refers to the magnitude of adsorption at t (min), and q_e (mg g^{-1}) indicates to the quantity of adsorption at equilibrium that can be calculated as in eq. 4.

$$q = \left(\frac{(C_0 - C_e)}{M}\right) \times V \quad (4)$$

Where C_0 and C_e is the initial and final dye concentration (mg L^{-1}), respectively, q_e is the amount of adsorbed concentration of dye (mg g^{-1}) on adsorbent, V is the volume of solution (L) and M is the mass of adsorbent used (g). Concerning conditions t = 0 to t = t and q = 0 to q = q_e a definite integration process was applied giving eq. 5.

$$\ln(q_e - q_t) = \ln q_e - k_1 t \quad (5)$$

Experimental estimation of adsorption rate constant, k, could be experimentally assessed by the slope of linear plots ln (q_e - q_t) vs. t. The slope of the straight line corresponds to the negative rate constant, $-k_1$, and the *y*-intercept corresponds to the natural logarithm of q_e. Concerning pseudo-second order model, Azizian (2004) summurized the kinetic process in eq. 6.

$$\frac{dt}{dq} = k_2(q_e - q_t)^2 \quad (6)$$

Where; k_2 (g mg^{-1} min^{-1}) is the rate constant of the pseudo-second order. Integrating precious equation for the limiting conditions t = 0 to t = t and q = 0 to q = e q_e illustrated in eq. 7.

$$\frac{1}{(q_e - q_t)} = \frac{1}{q_e} + k_2 t \quad (7)$$

Which has a linear form of eq. 8

$$\frac{t}{q_t} = \frac{1}{k_2 q_e^2} + \frac{1}{q_e} t \quad (8)$$

K_2 and q_e can be obtained from the intercept and slope of plotting t/q_t vs. t. k_2 and q_e can be obtained from the intercept and slope of plotting t/q_t vs. t. The slope of the straight line corresponds to $1/q_e$, and the *y*-intercept corresponds to $slope^2/k$ (Ho, 2006).

Adsorption isotherms

For solid-liquid system, the equilibrium of sorption is one of essential physico-chemical characteristics in explanation of bioadsorption behaviour, so that Langmuir and Freundlich models were studied as described by Vijayaraghavan et al. (2006) and Hernández-Zamora et al. (2015).

Langmuir adsorption isotherm

Langmuir isotherm is effective for monolayer adsorption onto a surface containing a finite number of identical sites. The linearized form of Langmuir is presented by eq. 9.

$$\frac{1}{q_e} = \frac{1}{Q_0} + \frac{1}{Q_0 K_L C_e} \quad (9)$$

Where C_e is the equilibrium concentration of adsorbate (mg L^{-1}), q_e is the amount of dye adsorbed per gram of the adsorbent at equilibrium (mg g^{-1}), Q_o is maximum monolayer coverage capacity (mg g^{-1}) and K_L is Langmuir isotherm constant (L mg^{-1}).

The magnitudes of Q_{max} and K_L were computed from the slope and intercept of the Langmuir plot of $1/q_e$ versus $1/C_e$ (Langmuir, 1918), where the intercept equals to $1/Q_{max}$ and the slope equals to $1/ (K_L Q_{max})$.

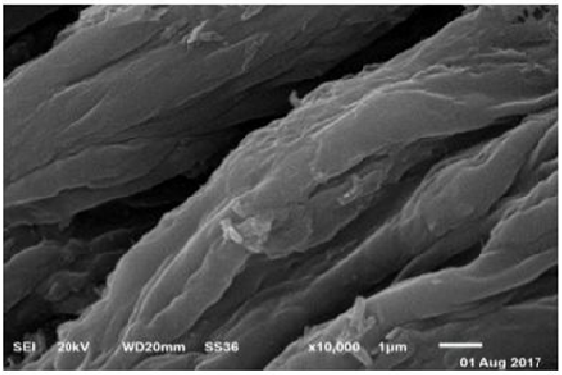

2.(a)

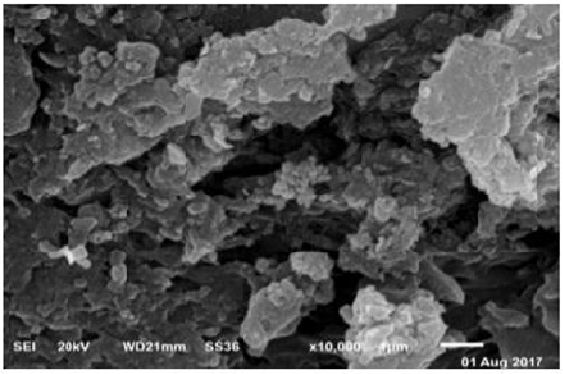

2.(b)

Figure 2 Scanning electron micrograph (SEM) of *N. carneum* biosorbent (a) before and (b) after MO loading

The essential feature of Langmuir isotherm may be expressed in terms of equilibrium R_L, which is a dimensionsless constant referred to as separation factor or equilibrium parameter as demonstrated by Weber and Chakravorti (1974) as in eq.10.

$$R_L = \frac{1}{1+(K_L C_0)} \quad (10)$$

Where C_o is the initial concentration and K_L is the constant associates to the adsorption energy (Langmuir constant). RL value demonstrate the adsorption nature to be either unfavorable (if $R_L > 1$) or linear (if $R_L = 1$) or favorable (if $0 < R_L < 1$) or irreversible (if $R_L = 0$) as reported by Chieng et al. (2015).

Freundlich Adsorption Isotherm

The well known logarithmic Freundlich model is given by the following linear form equation:

$$Log\, q_e = Log\, K_f + \frac{1}{n_f} Log\, C_e \quad (11)$$

Where K_f is Freundlich isotherm constant related to the adsorption capacity (mg g^{-1}), n is adsorption intensity or surface heterogeneity, C_e is the equilibrium concentration of adsorbate (mg L^{-1}) and q_e is the amount of metal adsorbed per gram of the adsorbent at equilibrium (mg g^{-1}). The values K_f and 1/n are calculated from intercept and slope of linear plot of log q_e versus log C_e (Intercept = log K_f and slope = 1/n). The magnitude of the exponent 1/n gives an indication of the favourability and capacity of the adsorbent/adsorbate system. Chieng et al. (2015) indicated that, when the magnitude of 1/n ranged from 0 to 1 the adsorption process is homogenous and characterized by absence of interaction among the adsorbed species when 1/n = 1 and the adsorption is unfavorable when 1/n > 1.

RESULTS AND DISCUSSION

Characterization of *N. carneum* biosorbent

Scanning Electron Microscopy (SEM)

The surface topology of the biosorbent ,*N. carneum,* before and after loading of MO indicated by scanning electron micrographs are illustrated in Figure. 2. The surface features revealed linear grooves and protrusions, which led to appropriate MO adsorption *via* increasing the surface area as described by Kiran et al. (2016). Figure. 2b shows the morphological changes onto *N. carneum* surface after loading of MO, which accumulated with different shapes and sizes. This feature may be resulted from the monolayer formation of MO molecules over the sorbent surface. This pattern of aggregations may interpret the high affinity of the cyanobacteria to the azo dye, confirming the efficiency of the biosorption process (Mahmoud et al. (2017). Fakhry (2013) documented that the variation in adsorption abilities of various groups algae might be incorporated to the morphological and compositional alterations of the cell walls.

X-ray diffraction (XRD)

X-ray diffraction technique is considered as a good investigation tool to detect the crystalline nature of the solid sorbents. Figures. 3a, 3b illustrate the XRD diffractogram of dried *N. carneum* biosorbent free and loaded with MO, respectively. XRD profile revealed the characteristic diffraction peaks corresponding to 2Θ= 25.1º, 29.3º, 31.6 º, 33.8 º and 45.4 º inter-planar spacing (d-spacing) 3.55045, 3.04940, 2.82801, 2.65088 and 1.99549 for the free

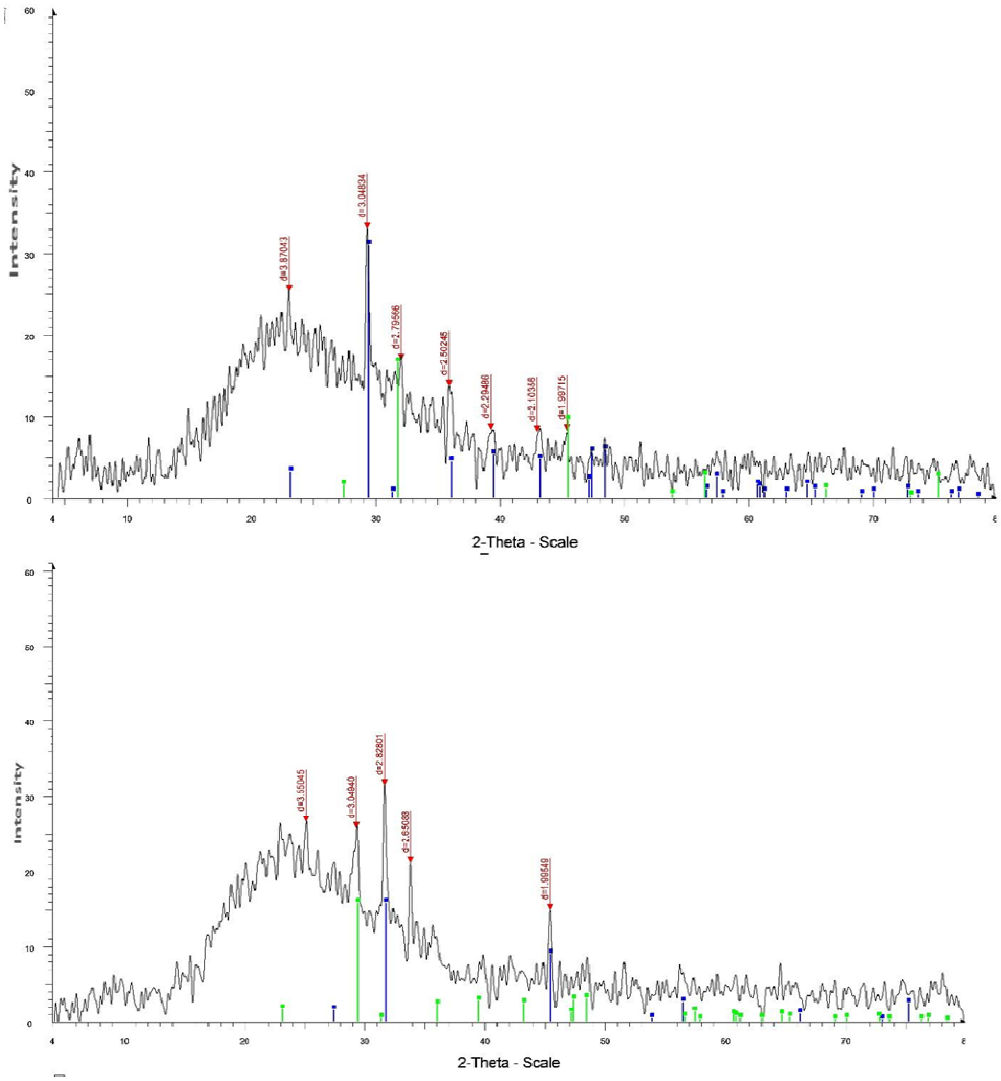

Figure 3: XRD pattern of (a) dried free (b) methyl orange loaded *N. carneum* biosorbent

biosorbent. Respecting the loaded biosorbent with MO, the diffraction peaks at 2Θ= 23º, 29.3º, 32º, 35.9º, 39.2º, 43º and 45.4º with inter-planar spacing (d-spacing) 3.87043, 3.04834, 2.79566, 2.50245, 2.29486, 2.10356 and 1.99715 Å . However, the comparable peak positions and intensity values with appearance of two new peak positions which indicated changes in the crystallinity of the sorbent after the adsorption process. XRD pattern of the free and loaded *N. carneum* biosorbent exhibit a shallow, broad and non-defined beaks indicating non-crystalline or amorphous nature as explained by Namasivayam and Kavitha (2006).

FT-IR analysis

FTIR spectroscopy provides essential data for the identification of the organic function groups of the surface of biosorbent, which are responsible for the interaction with MO, i.e, the binding sites available for the biosorption as explained by Natarajan and Ponnaiah (2017). FTIR profile distribution of protein and carbohydrates for *N. carneum* biomass before and after MO adsorption are illustrated in Figure. 4. Kelewou et al. (2014). Biosorption of textile dyes basic yellow 2 (BY2) and basic green 4 (BG4) by the living *Saccharomyces cerevisiae* cells showed that the adsorption may be attributed to the cell surface active groups of some cellular components of the cell wall as polysaccharides, lipids, amino acids as well as phosphoryl and carboxyl groups. In both loaded and unloaded biosorbent, the aliphatic hydrocarbons represented by methylene groups vas(C-H) stretching at 2923 cm^{-1} while that at 2853 cm^{-1} referred to vs(C-H) stretching of aldehydes and ketones (Suart, 2004). The bands at 1405 and 1408 cm^{-1} in loaded and unloaded biosorbent represented the bending of the methylene group (=C-H) as

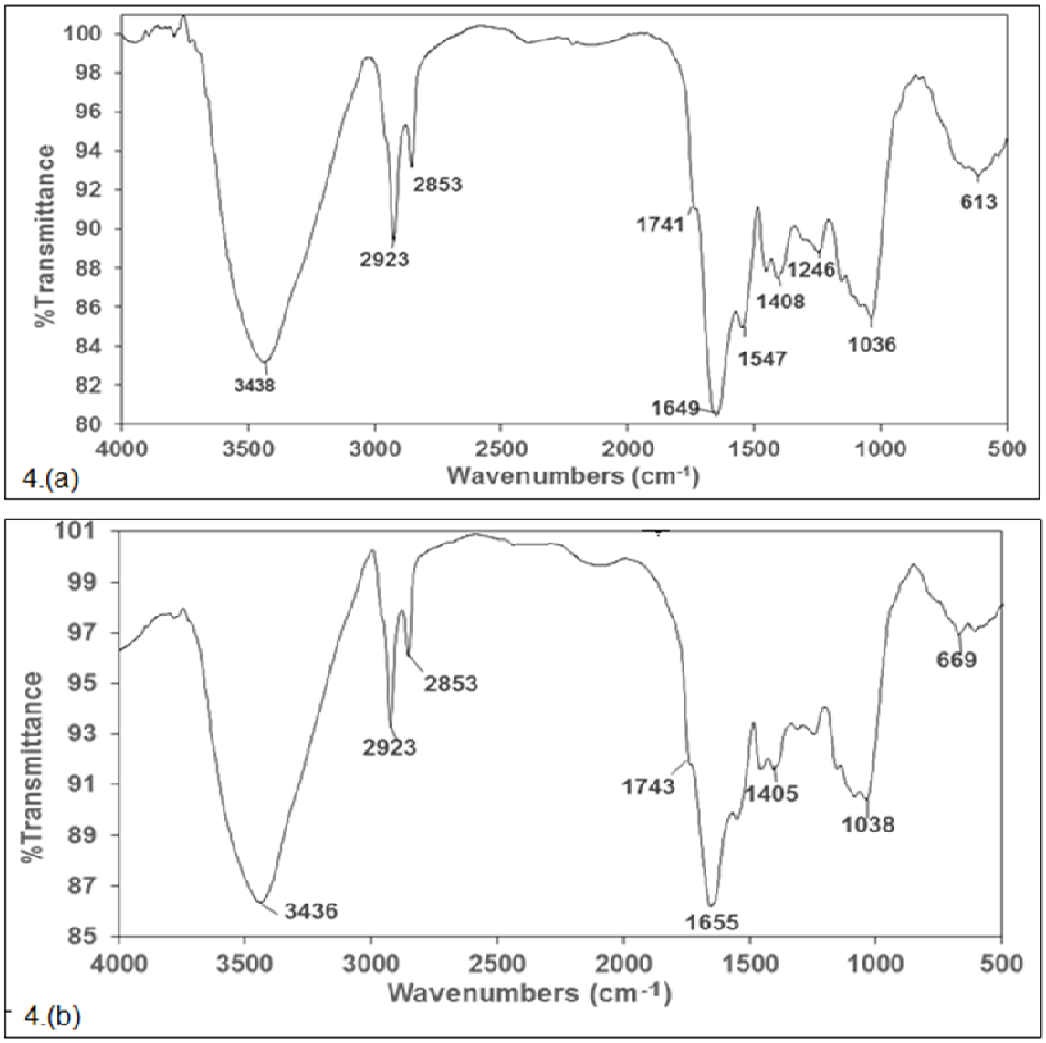

Figure 4 FT-IR spectra of (a) free *N. carneum* biosorbent and (b) *N. carneum* biosorbent loaded by methyl orange

well as it could be assigned to secondary amide C=O stretching as indicated by Suart (2004) and Chandrasekhar and Pramada (2006). Therefore, the band at 1649 cm^{-1} that attributed to vs(C=C) stretching vibration of alkenes, that was shifted to 1655 cm^{-1} (Ahmad and Kumar, 2010). Suart (2004) suggested that in the 2000 - 1700 cm^{-1} area, a group of weak combination and overtone beaks at 1741 cm^{-1} in the free biosorbent and shifted to 1743 cm^{-1} in the loaded one, referred to the aliphatic v(C=O) stretching of esters. Skeletal vibrations, representing v(C=C) stretch in the range 1650 – 1430 cm^{-1}, while the band at 1547 cm^{-1} could be assigned to aliphatic nitro-compound vas(NO_2) as suggested by Suart (2004). The bands at 1036 and 1038 cm^{-1} could be attributed to the aromatic C-H bending beak located at the infrared region of 1275 – 1000 cm^{-1} of the unloaded and loaded biosorbents. This could be also attributed to phosphorus ester P-OH stretching overlapping with S=O stretching (Suart, 2004). After dye loading, the broad peak at 3438 cm^{-1} is shifted to 3436 cm^{-1} which referred to the overlapping of O–H and N–H stretches (amines); i.e., the existence of both surface free hydroxy groups and chemisorbed water on the biosorbent which agreed with Sarı and Tuzen (2008). The presence of the band at 1246 cm^{-1} could be attributed to the presence of aromatic P-O stretchg in the unloaded biosorbent and disappeared after loading. The shift of band at 613 cm^{-1} to 669 cm^{-1} is due to the overlapping of =C-H bending alkynes with C-S stretching for both unloaded and loaded biosorbent, respectively (Suart, 2004). The shift in wave numbers after dye loading might be appeared due to the presence of amide, hydroxyl, carboxylate and C–O groups, that seem to be involved in MO adsorption on the cell surface of *N. carneum*; i.e., according to variation in bonding energy in the corresponding function groups. Little

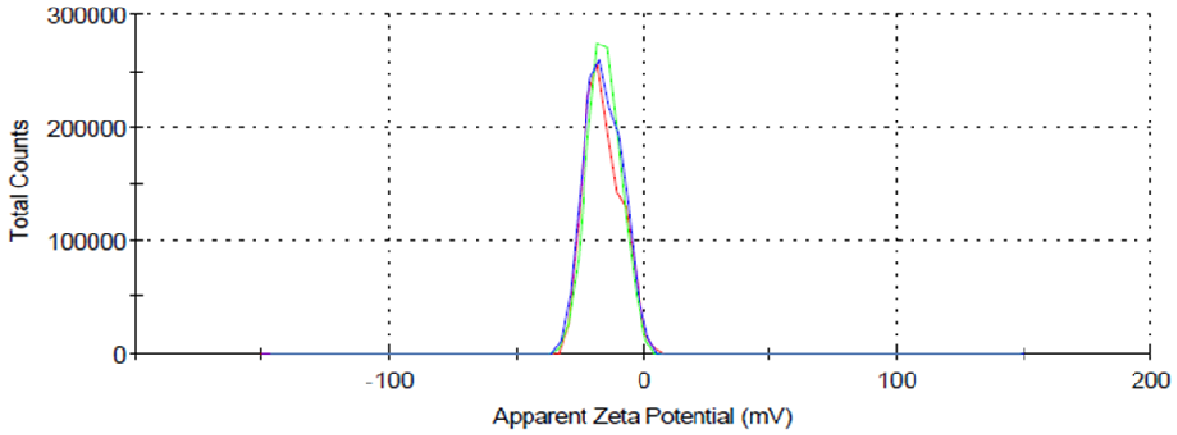

Figure 5 Zeta potential of fresh *N. carneum* aqueous extract

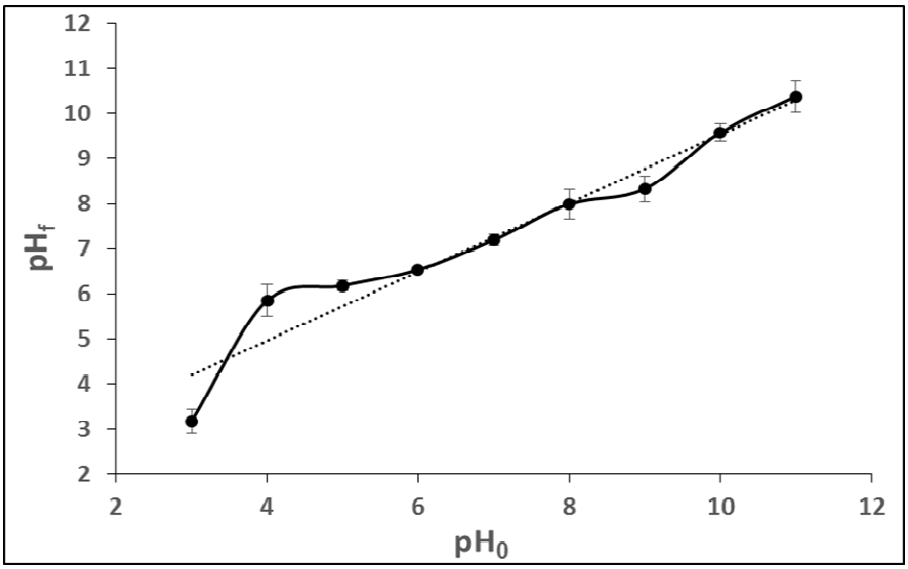

Figure 6 Changes in biosorbent pH after 24 hours incubation (pH_0 vs. pH_f)

probability of any biodegradation of the dye during the biosorption process was explained according to lack of any observed new peaks or major changes after MO loading as suggested by Daneshvar et al. (2007). The presence of the previously mentioned chemical groups indicated that *N. carneum* biosorbent characterized with a heterogeneous surface containing various classes of adsorption positions. These sites might give the prediction of cell wall nature as well as its response to MO molecules binding mechanism as concluded from Aksu and Tezer (2005), Chojnacka et al. (2005), Şeker et al. (2008) and Crist et al. (1981) suggested that amines, carboxylates, imidazols, phosphates, sulphates, sulfhydryls and hydroxy were positively charged when protonated composing the main binding groups of algae. Fakhry (2013) have reported that both carboxy and hydroxyl groups were the main responsible for the azo dye (acid fast yellow) biosorption onto *Padina* biomass, this finding is in agreement with these of Murphy et al. (2007). Peptidoglycans of bacteria and cyanobacteria represent one of the most effective binders of investigated metals (Noreen et al., 2013).

Zeta potential measurement

The zeta potential measurement of the *N. carneum* aqueous extract showed electro negativity quantified to -15.5 mV (Figure. 5) and the zero point charge was tested between the initial pH (pH_0) and final pH (pH_f) , giving pH 7 (Figure. 6). Daneshvar et al. (2007) as well as Kyzas et al. (2012) put their explanation depending on the zero point

charge for algal biomass. The negative charge of biomass surface for pH higher than zero point charge improves dye cations that have positive charge over electrostatic attraction force. The ionization of the different functional chemical groups of the alga organic matter could be responsible for the documented negativity (Pivokonsky et al., 2016). The variation in results might be depended on different algal strength cultures compositions as suggested by Kam and Gregory (2001). For pH lower than zero point, the charge of the surface becomes positive that forcing protons ions to struggle the dye cation for biosorption sites resulting in a reduction of the dye decolorization efficiency (Kumar and Ahmad, 2011; Tsai and Chen, 2010). Çelekli et al. (2011) studied the predictive modelling of biosorption of Lanaset Red G onto the macrochlorophyte *Chara contraria.* The zero point charge (pH_{zpc}) of *C. contraria* is 7.9 pH. Owing to lowering in pH values less than pH_{zpc}, the positivity of the macro-algae surface could be generated, so that sorption capacity towards anionic dyes could be increased according to the electrostatic attraction. In contrast, electrostatic repulsion could limit the sorption ability at pH higher than pH_{zpc}. Thus, the raising of biosorption capacity of *C. contraria* at pH 1 was attributed to the presence of additional positively charged functional groups that showed strong electrostatic attractions on anionic dyes.

Adsorption kinetics

In respect to kinetic modelling, allocation of solute molecules to the surface particle sorbent particle surface, transfer from the sorbent surface to the intraparticle active sites and retention on these active sites *via* adsorption, complexation or intraparticle precipitation phenomena, are the factors that controlled the adsorption kinetics (Noreen et al., 2013; Safa and Bhatti, 2011; Shroff and Vaidya, 2011). Adsorption is a time-dependent process and It is essential to assess the adsorption rate for evaluating the system efficiency (Aksu and Tezer, 2005). In order to study the mechanism of adsorption of MO onto the *cyanobacterial,* kinetic experiments were followed, where the pseudo-first order and pseudo-second order kinetics models were applied in order to match the experimental data. Yadav et al. (2013) supposed a chemosorption operation with a rate limiting one according to the pseudo-second-order kinetic model due to either the involvement of valance forces sharing or electrons exchange among the adsorbent and the adsorbate.

The adsorption kinetics were investigated by applying the two kinetic models; pseudo-first order and pseudo-second order by fitting the experimental data. The straight-line plots of ln (q_e-q_t) versus t for the pseudo-first order reaction and t/q_t versus t for the pseudo-second order reaction for adsorption of MO onto *Nostoc carneum* have also been

reported in Figure. 7. The kinetics data of *Nostoc carneum* treated with 5, 10, 20, 30, 40, 50, 60, 70 and 80 mg L^{-1} MO were analysed (Table 1)**.** The best models were designated by either the estimation of R^2 or comparing the adsorption potentiality values $q_{e,cal.}$ and $q_{e,exp}$**.** In order to determine the perfect kinetics model to explain the sorption operation of MO onto *N. carneum*, illustrated R^2 values of both kinetic models were indicated that pseudo second order model showed the highest value R^2 (0.99) for 50 mgL^{-1} concentration, recommending that this model gives the best correlation for the adsorption of MO on *N. carneum*. In addition, the $q_{e,cal.}$ value (769.23 mg g^{-1}) is well fitted ($q_{e,exp}$ 730.63 mg g^{-1}). According to Chu et al. (2009), biosorption is the effective mechanism in dye removal by microalsgae. Wang et al. (2016) reported that algae have an efficient biosorption potentiality because of their fast growth, high binding ability as well as high surfsce arae. Moreover, possesing of algal cell wall to numerourus chemical functional groups as sulphates, phosphates, imidazoles and carboxy connected to proteins, some cell wall polysaccharides, algenates, extracellular soluble polysaccarides (SPS).

The interrelation between SDR and initial dye concentration was clearly illusterated by the Michaelis–Menten model (Chen and Lin, 2007). 2.368 mg g^{-1} h^{-1} and 46.435 mg l^{-1} quantified the obvious maximum specific decolorization rate (SDR_{max}) as well as the Michaelise – Menten constant for initial dye concentration (Km), respectively.

Synthetic azo dyes have many different structures such as isomers or functional groups, which influence the decolorization potentiality through biodegradation and reduction. It has been reported that dyes with low molecular weights and simple structures reveal higher decolorization rate, while in the case of dyes with substituted electron withdrawing groups, i.e. $–SO_2NH_2$ and $–SO_3H$ in the para position of the phenyl ring, the rate of decolorization is decreased compared to the high molecular weight and azo dyes (Hsueh et al., 2009; Pearce et al., 2003). Rau and Stolz (2003) suggested that presence of hydroxy or amino groups in some azo dyes made them easily to degrade than those which possessed methyl, methoxy, sulpho or nitro groups. Reduction to the anion radical of azo dyes takes place *via* one-electron transfer reaction, secondly by slower electron transfer for supplying the stable dianion. According to higher electronic density, function groups, azo dyes could be not suitable for this second electron transfer forming the dianion, resulting in decrease in decolorization capacity as indicated by Pearce et al. (2003). Consequently, the sulfonated reactive group of azo dyes are regarded to be more recalcitrant than carboxylated azo dyes. Moreover, the diffusion of dyes *via* bacterial cell membrane was the limited step through sulfonated azo dyes adsorption onto bacterial biosorbent as explained by Kodam et al. (2005)**.**

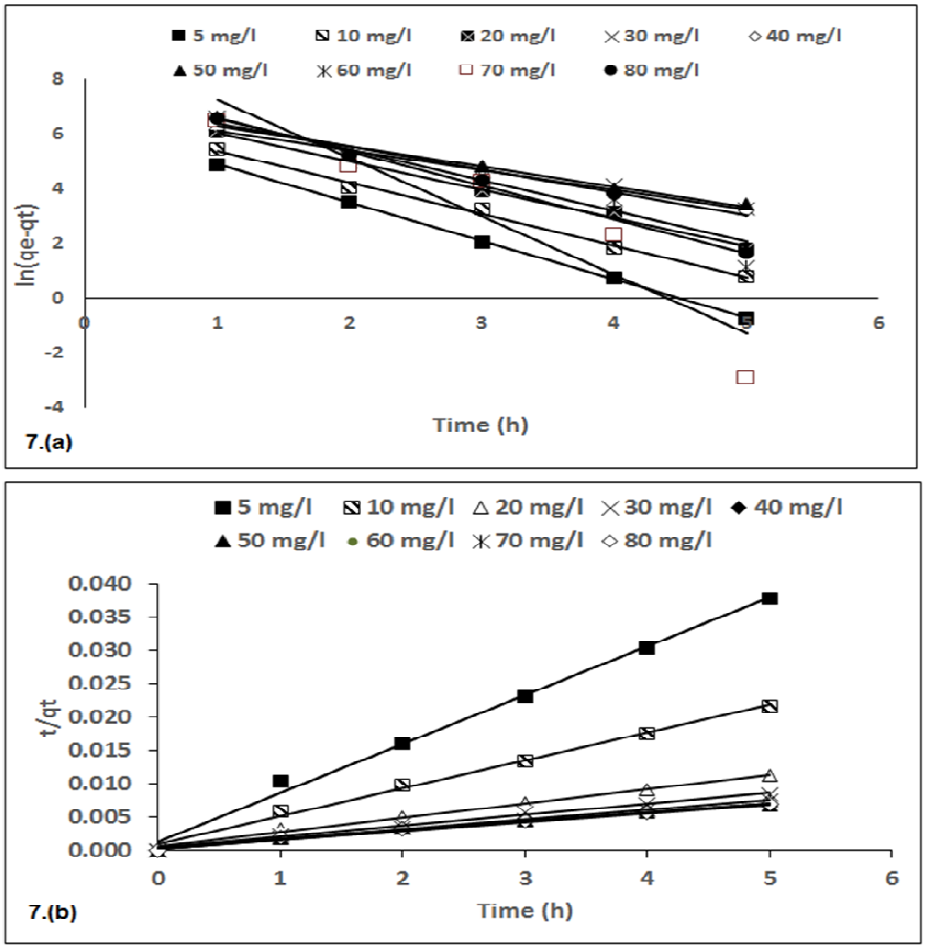

Figure 7 (a) Pseudo-first order kinetic plot and (b) Pseudo-second order kinetic plot for the MO biosorption by fresh *N. carneum* biomass at different MO initial concentrations (5, 10, 20, 30, 40, 50, 60, 70 and 80 mg l^{-1}

Table 1 Kinetic parameters for pseudo-first order and pseudo-second order models

C_0 (mg L^{-1})	Experim-ental q_e (mg g^{-1})	Pseudo-first order			Pseudo-second order		
		$q_{e\ cal.}$ (mg g^{-1})	k_1 (mg g^{-1} min^{-1})	R^2	$q_{e\ cal.}$ (mg g^{-1})	K_2 (mg g^{-1} min^{-1})	R^2
5	132.160	134.558	1.4000	0.999	136.986	0.0410	0.995
10	230.340	215.918	1.1460	0.994	238.095	0.0196	0.995
20	447.231	411.578	1.0304	0.992	454.545	0.0097	0.993
30	599.486	451.420	0.7206	0.953	625.000	0.0064	0.991
40	754.400	585.285	0.8325	0.974	769.231	0.0056	0.992
50	730.635	546.699	0.7467	0.955	769.231	0.0056	0.992
60	742.316	724.513	1.2377	0.943	769.231	0.0085	0.997
70	666.198	1435.834	2.1330	0.864	666.667	0.0113	0.997
80	718.355	707.473	1.1230	0.950	666.667	0.0065	0.994

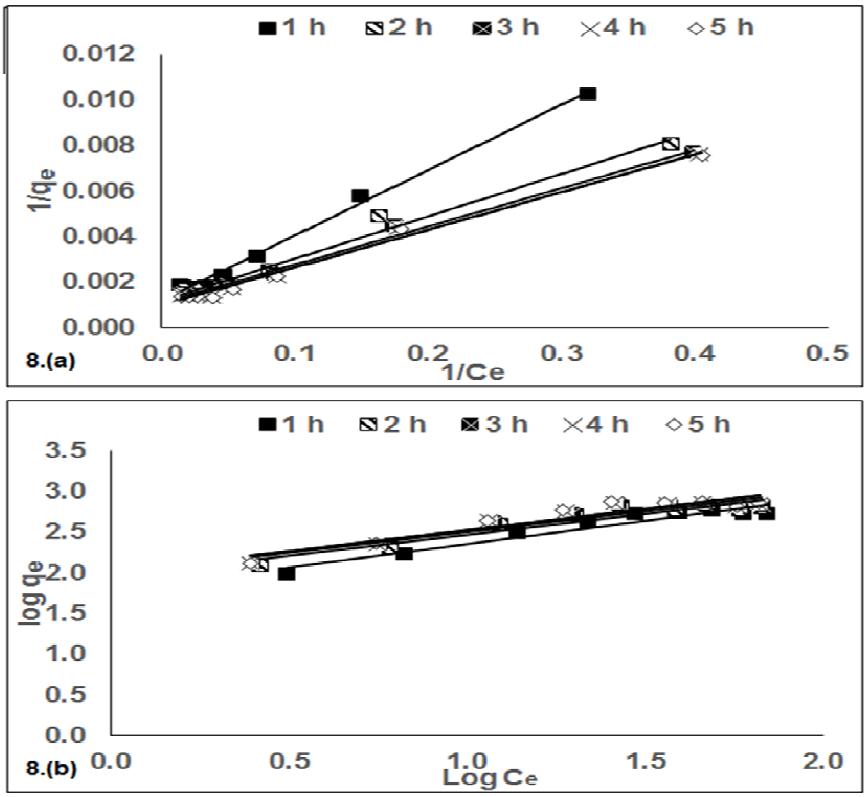

Figure 8 (a) Langmuir isotherm and (b) Freundlich for adsorption of methyl orange by fresh *N. carneum* biomass at different time (1, 2, 3, 4and 5 hours)

Adsorption isotherms

Adsorption isotherms are defined as the ratio between the amount adsorbed and the residual in solution at constant temperature at the case of equilibrium, since these studies reflect the potentiality of adsorbent and the equilibrium relationships between adsorbent and adsorbate (dye). The examination and strategy of dye biosorption operation are in need of significant adsorption equilibrium that give essential physiochemical records for assessing the dye biosorption application as documented by Srivastava and Rupainwar (2009). Isotherm equations have been applied for quantitative assessment of *N. carneum* fresh biomass and to explain the interaction of *N. carneum* fresh biomass and dye molecules. Different isotherm models such as Langmuir and Freundlich were applied.

In spite of having no explanation for the mechanism of adsorption, Langmuir adsorption isotherm study puts an interpretation of the uptake capabilities and any disorder in the equilibrium process manners. Linear Langmuir equation plot 1/qe versus 1/Ce was illustrated in Figure. 8(a). The value of isotherm constants (K_L, R_L) and equilibrium monolayer capacities, Q_m values are listed in Table 2. It is obvious that, high relation coefficient R^2 for all tested hours which equalled to 0.99 demonstrated the success of Langmuir isotherm model in interpretation of the adsorption process between MO and the biosorbent (*N. carneum* biomass) exhibiting a maximum adsorption capacity (Q_m) of 1027.71 mg g^{-1} after 5 hours. The assessment of R_L values of the adsorption process for the various biosorbate concentrations occupied values < 1 for all time intervals, indicating that the adsorption behavior of *N. carneum* biosorbent was adequate for MO. Data revealed that the adsorption isotherm supposed that there were rapid decrease in the intermolecular forces with distance expecting the existence of monolayer adsorbate at the external surface of the *N. carneum* biosorbent where adsorption occurs (Srivastava and Rupainwar, 2009).

Freundlich isotherm model based on a heterogeneous surface with a non-uniform distribution of adsorption. Linear Freundlich equation plot log qe versus log Ce was illustrated in Figure. 8(b). It was clarified that R^2 ranged between 0.93 and 0.95 and 1/ n (the heterogeneity factor) values lied between 0 and 1 at different time intervals (Table 2), indicating that the adsorption process is homogenous and characterized by absence of interaction among the adsorbed species (Mohanty et al., 2006). Relation coefficient (R^2) 0.99 of Langmuir proves a better choice in interpreting the biosorption reaction between MO

Table 2 Langmuir and Freundlich isotherm constants for the adsorption of methyl orange dye onto *N. carneum* biomass

Time (h)	Langmuir isotherm constants				Freundlich isotherm constants		
	Q_m (mg/g)	K_L (L mg^{-1})	R_L range	R^2	K_f (mg g^{-1})	1/n	R^2
1	851.52	0.0410	0.2544-0.8269	0.9972	60.379	0.5786	0.9592
2	852.57	0.0632	0.7556-0.1809	0.9906	88.861	0.5214	0.9474
3	923.57	0.0642	0.7540-0.1796	0.9950	97.804	0.5164	0.9506
4	988.54	0.0611	0.7680-0.1912	0.9946	100.502	0.5226	0.9465
5	1027.71	0.0590	0.7673-0.1906	0.9940	102.777	0.5227	0.9378

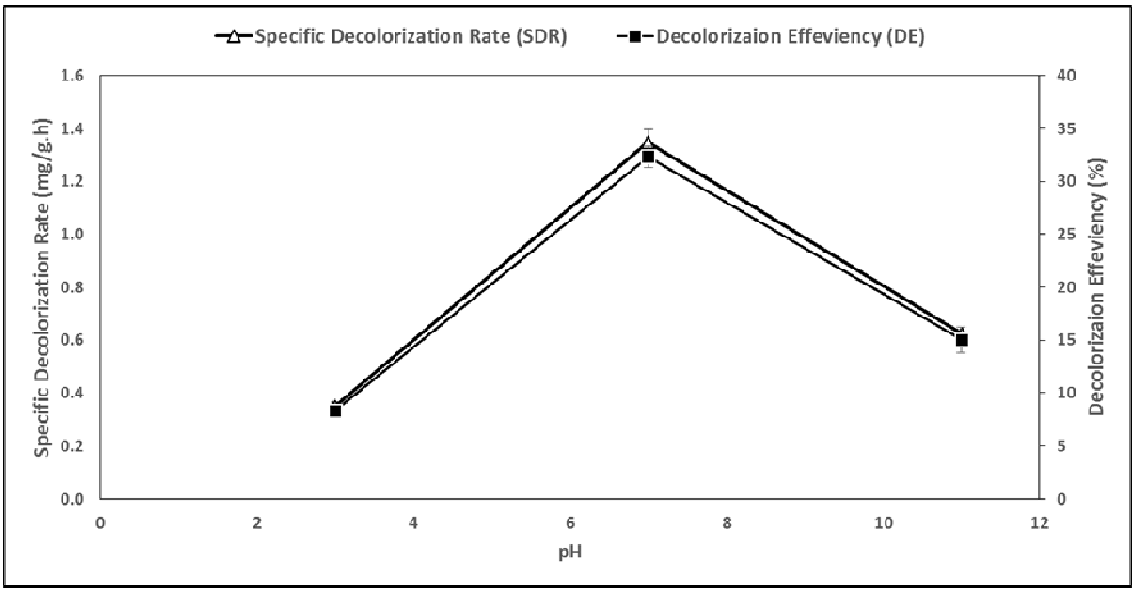

Figure 9 Dependence of specific decolorization rate (SDR) and decolorization efficiency (DE) of fresh *N. carneum* biomass (biosorbent) on initial different pH values using 50 mg l^{-1} as initial dye concentration

and *N. carneum* fresh biomass that is in agree with Tan et al. (2010) who studied the biosorbtion of basic organic (BO) textile dye onto dried cyanobacterium *Anabaena filiculoides*. In the same context, the adsorption of Remazol Red and Remazol Golden Yellow (reactive dyes) onto the microchlorophyte *Chlorella vulgaris* dried biomass is fitted to Langmuir model according to Aksu and Tezer (2005). Gong et al. (2007) studied the sorbent capacity of the rice straw modified product for removing both basic blue 9 (BB9) and red 5 (BR5) dyes from aqueous solution. They demonstrated the dependence of Langmuir equation on the hypothesis that highest level of sorption relates to a saturated monolayer of sorbate molecules on the sorbent surface. They ensure that the energy of sorption process is stable indicating no transmigration of the sorbate in the plane of the surface.

Factors affecting decolorization efficiency and specific decolorization rate

Effect of initial pH

MO removal criteria of *N. carneum* at various pH values of adsorbate solutions (pH 3, pH 7 and pH 11) was illustrated in Figure. 9. pH 7 was found to be the most favorable value for the decolorization which exhibited its maximum value revealing that dye biosorption is highly pH dependent bioprocess. The optimum pH value for dye decolorization efficiency (32.34 %) and specific decolorization rate (1.3473 mg g^{-1} h^{-1}) was obtained at pH 7. However, both acidic pH 3 and basic pH 11 exhibited low dye decolorization efficiency with 8.36% and 15.02%

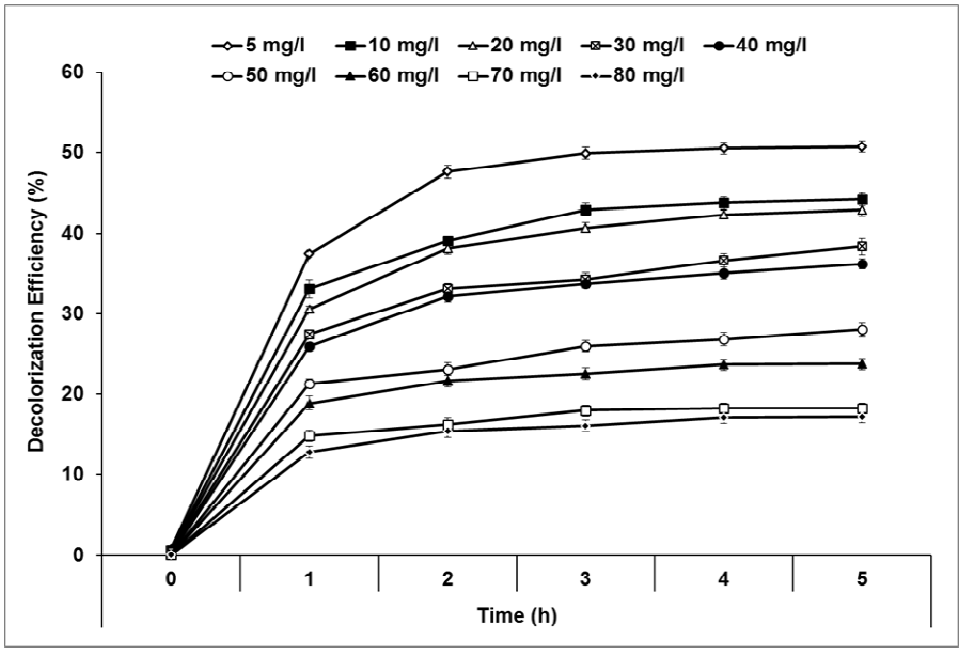

Figure 10 Effect of contact time on MO decolorization efficiency of different initial MO concentrations (5, 10, 20, 30, 40, 50, 60, 70 and 80 mg l^{-1}) by *N. carneum* fresh biomass

respectively, at 5 hours contact time. Value of pH of sorbate solution had been documented as a significant factor influencing biosorption operation according to its effect on the surface charge of biosorbent as well as dyes solubility as suggested by Çelekli et al. (2011). Shah et al. (2013) suggested that varying pH induced changes in the decolorization activity of bacteria, whereas, *Pseudomonas* spp. was able to reduce MO color through an extensive range of pH (6–10) demonstrating pH 8 (80% dye decolorization) as the optimum pH. They also found large decrease in decolorization activity occurs at high acidic pH (2–4) which is in accordance with the present results. In the same context, Tsai and Chen (2010) reviewed that the surface binding-sites of algal cell wall holds various functional groups like carboxyl, hydroxyl, sulphate and other charged group as well as the ionization or aggregation process of the dye molecules are influenced by the adsorbate solution pH.

Daneshvar et al. (2007) studied the reduction of malachite green color using the micro-chlorophyte *Cosmarium* sp. as biosorbent. They investigated the influence of pH values (from 2 to 11) on the decolorization process. They found that raising pH values from 4 to 6 causing high increments in decolorization rate, meanwhile pH 9 induced the maximum of decolorization. Nandi et al. (2009) suggested that pH is the main factor influencing adsorption process, since the surface charge showed the dependence of the availability of free sites on pH according to the surface charge of the adsorbent, the degree of ionization of the adsorptive molecule and extent of dissociation of functional groups on the active sites of the adsorbent.

Effect of initial dye concentrations

Adsorption batch experiments were carried out with different contact times (0 – 5 h) at constant adsorbent dose (fresh biomass of *Nostoc carneum* equivalent to 2.4 mg dry weight). Dye decolorization efficiency progressively increased with time as illustrated in Figure. 10. On the other hand, it was obviously showed in Figure. 11 that decolorization effeciency decreased while SRD increase with increasing MO concentration, which in agreement with Chen and Lin (2007). The uppermost values of decolorization efficiency percentage were established for the low initial dye concentrations of 5, 10 and 20 mg L^{-1}. After 5 h exposure, the decolorization efficiency of 50.749, 44.225 and 42.934 %, respectively. This is in accordance with Nandi et al. (2009), who explained the relation between contact time and the quantity of adsorbed dye onto adsorbent regarding to the time needed for reaching equilibrium. According to the interpretation of Kyzas et al. (2012), fast adsorption at the primery stage might be attributed to the accessability of large amount of surface sites for adsorption, leading to adsorption of MO molecules on the outward surface of the negatively charged *N. carneum* biomass through boundary layer adsorption. As expanding of contact time, the surface of the algal becomes saturated. Consequently, a limitation in number of surface sites of MO adsorption occurred because of the

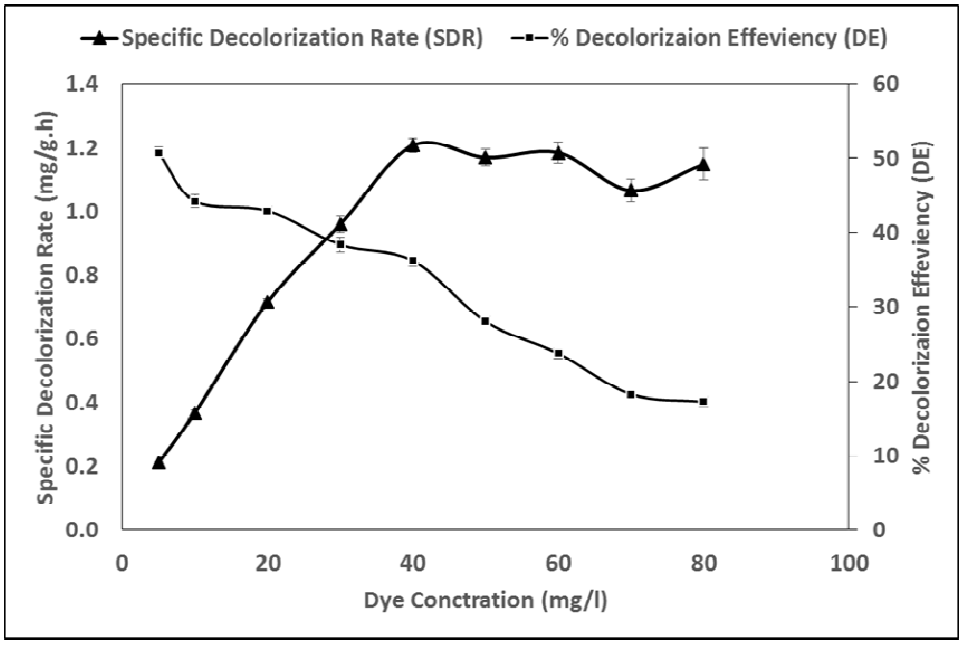

Figure 11 Dependence of specific decolorization rate (SDR) and decolorization efficiency (DE) of fresh *N. carneum* biomass (biosorbent) on the initial MO concentrations (5, 10, 20, 30, 40, 50, 60, 70 and 80 mg l^{-1})

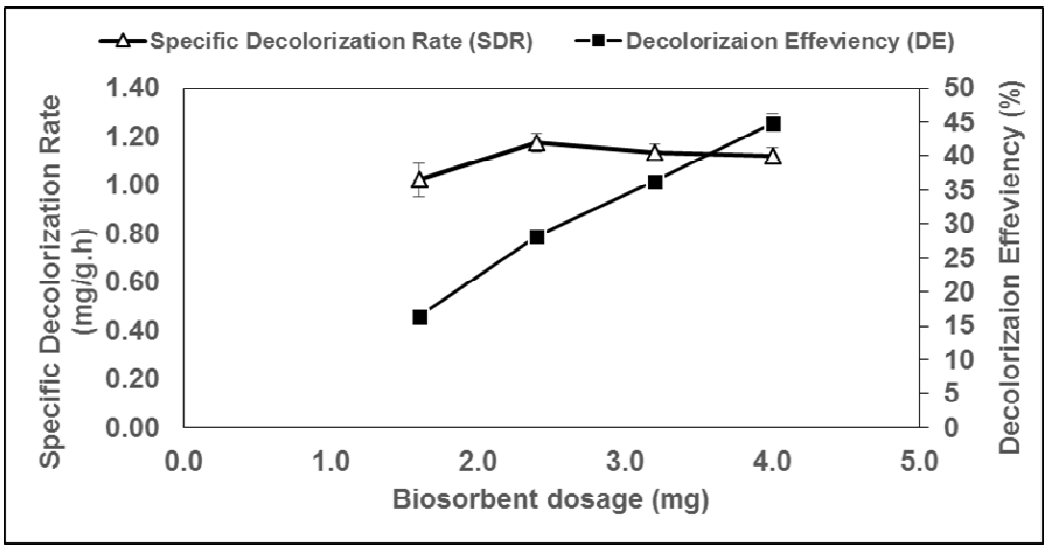

Figure 11 Dependence of specific decolorization rate (SDR) and decolorization efficiency (DE) of fresh *N. carneum* biomass on biosorbent dosage using 50 mg l^{-1} as initial MO concentration

existence of repulsive forces that found between MO molecules present on *N. carneum* cells and MO molecules present in the solution (Mane and Babu, 2011; Nandi et al., 2009). In the next stage, there is deep diffusion of MO molecules into the cell wall of *N. carneum*, that slow down the adsorption process which resulting in aggregation of MO molecules at the maximum contact time (Mane and Babu, 2011).

The maximum peak of adsorption equilibrium for the algal-MO approach became steady at 3 hours contact time (Figure. 11), since the engagement of a passive process for dye loading on cell external surface is followed by a gradual and slow stage associating with active energy mediated process as explained by Mona et al. (2011). In the same context for interpretting dye adsorption process, Malik (2003), indicated that dye molecules must diffuse to the border layer of the biosorbent firstly, then adsorbed

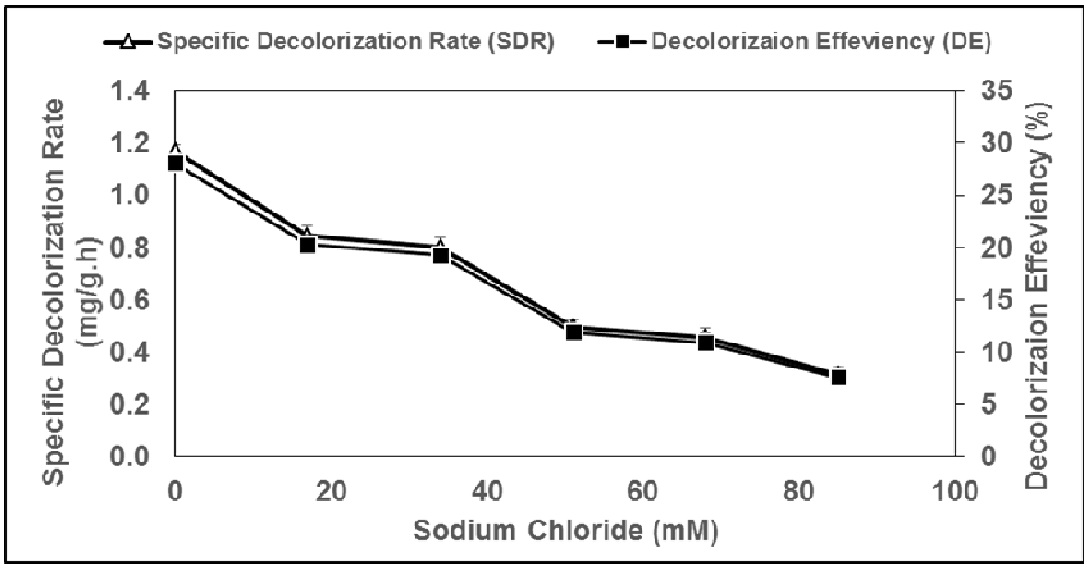

Figure 12 Dependence of specific decolorization rate (SDR) and decolorization efficiency (DE) of fresh *N. carneum* biomass (biosorbent) on different sodium chloride concentrations using 50 mg l^{-1} as initial MO concentration

onto the surface and lastly, difused into the porous structure of the biosorbent, a process which extented contact time. The rapidness of the initial phase might be atributed to the highest number adsorption sites at the beginning of the adsorption process, which creats an increased concentration gradient between MO molecules (adsorbate) in solution and the adsorbate in the adsorbent. Moreover, increasing initial dye concentration increases the number of collisions between dye anions and sorbent, which enhances the sorption process (Aksu and Tezer, 2005).

Effect of biosorbent dosage

The DE % is increased gradually with increasing biosorbent dosage (Figure. 12), while SDR showed the highest value with biosorbent dosage corresponding to 2.4 mg dry biomass. The biosorption of MO is increased with increasing the biosorbent dosage. These results could be attributed to the expansion of the adsorbent surface area as well as the availability of more adsorption sites as demonstrated by Waranusantigul et al. (2003) and Çelekli et al. (2012). Hernández-Zamora et al. (2015) found that increasing the dose of *Chlorella vulgaris* from 51 mg L^{-1} to 146 mg L^{-1} at different concentrations of Congo Red, inducing increments in dye adsorption and the amount of residual dye decreased significantly. Moreover, increasing CR concentration from 5 – 25 mg l^{-1}, induced reduction of the biosorption from 67 to 32 % for 51 mg l^{-1}. In general, when the specific decolorization rate was measured as mg g^{-1} h^{-1}, it would increase with decreasing in the biosorbent dosage as explained by Çelekli et al. (2012). This feature may be due to partial overlying and/or accumulation of biosorbent particles at higher doses of *N. carneum* leading to a reduction in the surface area and consequently biosorption sites availability.

Effect of ionic strength

N. cranium was tested for its ability to decolorize the MO dye in the presence of different concentrations of sodium chloride (17, 34, 51, 68 and 85 mM), which showed the highest specific decolorization rate was the minimum sodium chloride supplementation (17 mM) at 0.8458 mg g^{-1} h^{-1} that decreases with increasing salinity until reach 0.3154 mg g^{-1} h^{-1} for 85 mM Na Cl. Decolorization efficiency (DE) exhibit the same pattern of change as in SDR (Figure. 13). Nandi et al. (2009) reported that increasing salt concentration induced reduction in dye decolorization efficiency, with increasing ion strength, adsorption capacity decreased due to binding of the surface charges. Residual dye concentrations had the opposite pattern of DE response with contact time increasing.

CONCLUSION

This study indicates promising overview of using *N. carneum* as a low-cost, natural, sustainable biosorbent for the removal of MO from aqueous solutions. The active groups of biosorbent surface interact with MO. The maximum specific decolorization rate (2.1734 mg g^{-1} h^{-1}) was reached at pH 7 with adsorbent dose corresponding to

2.4 mg dry biomass with contact time 5 h. The adsorption process obey the pseudo first order kinetics Langmuir adsorption isotherm, which indicated that the monolayer adsorption has been taken place. Finally, it can be concluded that the potentiality *N. carneum* for MO biosorption depends on dye structure, concentration as well as the experimental conditions.

ACKNOWLEDGEMENT

The authors would like to thank The Electron Microscope Unit of Mansoura University in Egypt due to facilitate using Malvern Instruments Ltd for zeta potential study.

REFERENCES

Ahmad R, Kumar R (2010). Adsorption studies of hazardous malachite green onto treated ginger waste. Journal of environmental management. 91: 1032-1038.

Aksu Z, Tezer S (2005). Biosorption of reactive dyes on the green alga Chlorella vulgaris. Process biochemistry. 40: 1347-1361.

Azizian S (2004). Kinetic models of sorption: a theoretical analysis. Journal of colloid and Interface Science. 276: 47-52.

Çelekli A, Tanrıverdi B, Bozkurt H (2011). Predictive modeling of removal of Lanaset Red G on Chara contraria; kinetic, equilibrium, and thermodynamic studies. Chemical engineering journal. 169: 166-172.

Çelekli A, İlgün G, Bozkurt H (2012). Sorption equilibrium, kinetic, thermodynamic, and desorption studies of Reactive Red 120 on Chara contraria. Chemical engineering journal. 191: 228-235.

Chandrasekhar S, Pramada P (2006). Rice husk ash as an adsorbent for methylene blue—effect of ashing temperature. Adsorption. 12: 27-43.

Chen J-P, Lin Y-S (2007). Decolorization of azo dye by immobilized Pseudomonas luteola entrapped in alginate–silicate sol–gel beads. Process biochemistry. 42: 934-942.

Chieng HI, Priyantha N, Lim LB (2015). Effective adsorption of toxic brilliant green from aqueous solution using peat of Brunei Darussalam: isotherms, thermodynamics, kinetics and regeneration studies. RSC Advances. 5: 34603-34615.

Chojnacka K, Chojnacki A, Gorecka H (2005). Biosorption of Cr 3+, Cd 2+ and Cu 2+ ions by blue–green algae Spirulina sp.: kinetics, equilibrium and the mechanism of the process. Chemosphere. 59: 75-84.

Chu W-L, See Y-C, Phang S-M (2009). Use of immobilised Chlorella vulgaris for the removal of colour from textile dyes. Journal of Applied Phycology. 21: 641.

Crist RH, Oberholser K, Shank N, Nguyen M (1981). Nature of bonding between metallic ions and algal cell walls. Environmental Science & Technology. 15: 1212-1217.

Daneshvar N, Ayazloo M, Khataee A, Pourhassan M (2007). Biological decolorization of dye solution containing Malachite Green by microalgae Cosmarium sp. Bioresource technology. 98: 1176-1182.

El-Sheekh MM, Gharieb M, Abou-El-Souod G (2009). Biodegradation of dyes by some green algae and cyanobacteria. International Biodeterioration & Biodegradation. 63: 699-704.

Fakhry EM (2013). Padina pavonica for the removal of dye from polluted water. American Journal of Plant Sciences. 4: 1983.

Gong R, Jin Y, Chen J, Hu Y, Sun J (2007). Removal of basic dyes from aqueous solution by sorption on phosphoric acid modified rice straw. Dyes and Pigments. 73: 332-337.

Heiss GS, Gowan B, Dabbs ER (1992). Cloning of DNA from a Rhodococcus strain conferring the ability to decolorize sulfonated azo dyes. FEMS microbiology letters. 99: 221-226.

Hernández-Zamora M, Cristiani-Urbina E, Martínez-Jerónimo F, Perales-Vela HV, Ponce-Noyola T, del Carmen Montes-Horcasitas M, Cañizares-Villanueva RO (2015). Bioremoval of the azo dye Congo Red by the microalga Chlorella vulgaris. Environmental Science and Pollution Research. 22: 10811-10823.

Ho Y-S (2006). Second-order kinetic model for the sorption of cadmium onto tree fern: a comparison of linear and non-linear methods. Water Research. 40: 119-125.

Hsueh C-C, Chen B-Y, Yen C-Y (2009). Understanding effects of chemical structure on azo dye decolorization characteristics by Aeromonas hydrophila. Journal of hazardous materials. 167: 995-1001.

Jinqi L, Houtian L (1992). Degradation of azo dyes by algae. Environmental pollution. 75: 273-278.

Kam S-K, Gregory J (2001). The interaction of humic substances with cationic polyelectrolytes. Water Research. 35: 3557-3566.

Kelewou H, Merzouki M, Lhassani A (2014). Biosorption of textile dyes Basic Yellow 2 (BY2) and Basic Green 4 (BG4) by the live yeast Saccharomyces Cerevisiae. J. Mater. Environ. 5: 633-640.

Kiran B, Rani N, Kaushik A (2016). FTIR spectroscopy and scanning electron microscopic analysis of pretreated biosorbent to observe the effect on Cr (VI) remediation. International journal of phytoremediation. 18: 1067-1074.

Kodam K, Soojhawon I, Lokhande P, Gawai K (2005). Microbial decolorization of reactive azo dyes under aerobic conditions. World Journal of Microbiology and Biotechnology. 21: 367-370.

Kumar R, Ahmad R (2011). Biosorption of hazardous crystal violet dye from aqueous solution onto treated ginger waste (TGW). Desalination. 265: 112-118.

Kyzas GZ, Lazaridis NK, Mitropoulos AC (2012). Removal of dyes from aqueous solutions with untreated coffee residues as potential low-cost adsorbents: Equilibrium, reuse and thermodynamic approach. Chemical engineering journal. 189: 148-159.

Langmuir I (1918). The adsorption of gases on plane surfaces of glass, mica and platinum. Journal of the American Chemical society. 40: 1361-1403.

Mahmoud MS, Mostafa MK, Mohamed SA, Sobhy NA, Nasr M (2017). Bioremediation of red azo dye from aqueous solutions by Aspergillus niger strain isolated from textile wastewater. Journal of Environmental Chemical Engineering. 5: 547-554.

Malik PK (2003). Use of activated carbons prepared from sawdust and rice-husk for adsorption of acid dyes: a case study of Acid Yellow 36. Dyes and Pigments. 56: 239-249.

Mane VS, Babu PV (2011). Studies on the adsorption of Brilliant Green dye from aqueous solution onto low-cost NaOH treated saw dust. Desalination. 273: 321-329.

Mohan SV, Bhaskar YV, Karthikeyan J (2004). Biological decolourisation of simulated azo dye in aqueous phase by algae Spirogyra species. International journal of environment and pollution. 21: 211-222.

Mohanty K, Jha M, Meikap B, Biswas M (2006). Biosorption of Cr (VI) from aqueous solutions by Eichhornia crassipes. Chemical engineering journal. 117: 71-77.

Mona S, Kaushik A, Kaushik C (2011). Waste biomass of Nostoc linckia as adsorbent of crystal violet dye: optimization based on statistical model. International Biodeterioration & Biodegradation. 65: 513-521.

Murphy V, Hughes H, McLoughlin P (2007). Cu (II) binding by dried biomass of red, green and brown macroalgae. Water Research. 41: 731-740.

Namasivayam C, Kavitha D (2006). IR, XRD and SEM studies on the mechanism of adsorption of dyes and phenols by coir pith carbon from aqueous phase. Microchemical Journal. 82: 43-48.

Nandi B, Goswami A, Purkait M (2009). Removal of cationic dyes from aqueous solutions by kaolin: kinetic and equilibrium studies. Applied Clay Science. 42: 583-590.

Natarajan E, Ponnaiah GP (2017). Optimization of process parameters for the decolorization of Reactive Blue 235 dye by barium alginate immobilized iron nanoparticles synthesized from aluminum industry waste. Environmental Nanotechnology, Monitoring & Management. 7: 73-88.

Noreen S, Bhatti HN, Nausheen S, Sadaf S, Ashfaq M (2013). Batch and fixed bed adsorption study for the removal of Drimarine Black CL-B dye from aqueous solution using a lignocellulosic waste: A cost affective adsorbent. Industrial Crops and Products. 50: 568-579.

Omar HH (2008). Algal decolorization and degradation of monoazo and diazo dyes. Pak J Biol Sci. 11: 1310-1316.

Ong S-A, Uchiyama K, Inadama D, Ishida Y, Yamagiwa K (2010). Treatment of azo dye Acid Orange 7 containing wastewater using up-flow constructed wetland with and without supplementary aeration. Bioresource technology. 101: 9049-9057.

Pearce C, Lloyd J, Guthrie J (2003). The removal of colour from textile wastewater using whole bacterial cells: a review. Dyes and Pigments. 58: 179-196.

Pinheiro H, Touraud E, Thomas O (2004). Aromatic amines from azo dye reduction: status review with emphasis on direct UV spectrophotometric detection in textile industry wastewaters. Dyes and Pigments. 61: 121-139.

Pivokonsky M, Naceradska J, Kopecka I, Baresova M, Jefferson B, Li X, Henderson R (2016). The impact of algogenic organic matter on water treatment plant operation and water quality: A review. Critical Reviews in Environmental Science and Technology. 46: 291-335.

Rakhshaee R, Giahi M, Pourahmad A (2011). Removal of methyl orange from aqueous solution by Azolla filicoloides: synthesis of Fe 3 O 4 nano-particles and its surface modification by the extracted pectin of Azolla. Chinese Chemical Letters. 22: 501-504.

Rau J, Stolz A (2003). Oxygen-insensitive nitroreductases NfsA and NfsB of Escherichia coli function under anaerobic conditions as lawsone-dependent azo reductases. Applied and Environmental Microbiology. 69: 3448-3455.

Safa Y, Bhatti HN (2011). Kinetic and thermodynamic modeling for the removal of Direct Red-31 and Direct Orange-26 dyes from aqueous solutions by rice husk. Desalination. 272: 313-322.

Sarı A, Tuzen M (2008). Biosorption of cadmium (II) from aqueous solution by red algae (Ceramium virgatum): equilibrium, kinetic and thermodynamic studies. Journal of hazardous materials. 157: 448-454.

Şeker A, Shahwan T, Eroğlu AE, Yılmaz S, Demirel Z, Dalay MC (2008). Equilibrium, thermodynamic and kinetic studies for the biosorption of aqueous lead (II), cadmium (II) and nickel (II) ions on Spirulina platensis. Journal of hazardous materials. 154: 973-980.

Shah M, Patel K, Nair S, Darji A (2013). Microbial decolourization of methyl orange dye by Pseudomonas spp. OA Biotechnology. 2: 10.

Shroff KA, Vaidya VK (2011). Kinetics and equilibrium studies on biosorption of nickel from aqueous solution by dead fungal biomass of Mucor hiemalis. Chemical engineering journal. 171: 1234-1245.

Srivastava R, Rupainwar D (2009). Eucalyptus bark powder as an effective adsorbent: Evaluation of adsorptive characteristics for various dyes. Desalination and Water Treatment. 11: 302-313.

Stanier R, Kunisawa R, Mandel M, Cohen-Bazire G (1971). Purification and properties of unicellular blue-green algae (order Chroococcales). Bacteriological reviews. 35: 171.

Suart B (2004). Infrared Spectroscopy: Fundamental and Applications. John Wiley & Sons, Ltd.

Tan C-y, Li G, Lu X-Q, Chen Z-l (2010). Biosorption of Basic Orange using dried A. filiculoides. Ecological Engineering. 36: 1333-1340.

Tsai W-T, Chen H-R (2010). Removal of malachite green from aqueous solution using low-cost chlorella-based biomass. Journal of hazardous materials. 175: 844-849.

Vijayaraghavan K, Padmesh T, Palanivelu K, Velan M (2006). Biosorption of nickel (II) ions onto Sargassum wightii: application of two-parameter and three-parameter isotherm models. Journal of hazardous materials. 133: 304-308.

Wang Y, Ho S-H, Cheng C-L, Guo W-Q, Nagarajan D, Ren N-Q, Lee D-J, Chang J-S (2016). Perspectives on the feasibility of using microalgae for industrial wastewater treatment. Bioresource technology. 222: 485-497.

Waranusantigul P, Pokethitiyook P, Kruatrachue M, Upatham E (2003). Kinetics of basic dye (methylene blue) biosorption by giant duckweed (Spirodela polyrrhiza). Environmental pollution. 125: 385-392.

Weber TW, Chakravorti RK (1974). Pore and solid diffusion models for fixed□bed adsorbers. AIChE Journal. 20: 228-238.

Yadav S, Srivastava V, Banerjee S, Weng C-H, Sharma YC (2013). Adsorption characteristics of modified sand for the removal of hexavalent chromium ions from aqueous solutions: Kinetic, thermodynamic and equilibrium studies. Catena. 100: 120-127.